CHARACTERIZATION OF ACTIVATED CARBON FIBERS

A. W. P. FUNG*, A. M. RAO**, K. KURIYAMA**, M. S. DRESSELHAUS*,**, G. DRESSELHAUS† AND M. ENDO‡

* Department of Electrical Engineering, Massachusetts Institute of Technology, Cambridge, MA

** Department of Physics, Massachusetts Institute of Technology, Cambridge, MA

† Francis Bitter National Magnet Laboratory, Massachusetts Institute of Technology, Cambridge, MA

‡ Faculty of Engineering, Shinshu University, Nagano, Japan

Abstract

Low-temperature electrical conductivity and Raman scattering are studied as characterization tools for activated carbon fibers, which have a high density of defects and a huge specific surface area. The transport mechanism at low temperature is governed by variable-range hopping, as in other strongly disordered systems. From the Raman spectra obtained, we deduce that the long phenolic fibers are more disordered than the acrylic fibers and that increased specific surface area corresponds to increased disorder. The average in-plane microcrystallite size is about 20–30 $\AA$.

Introduction

Although the adsorption properties of activated carbons have been extensively studied, there has been little work done on other physical properties of this interesting material, which possesses an unusally high density of defects and a huge specific surface area (SSA), exceeding that in other solids. The recent success in the fabrication of activated carbon fibers (ACFs) allows the transport properties of this disordered material to be investigated. Di Vittorio [1] has made a preliminary survey of the temperature dependence of the dc electrical conductivity, the magnetoresistance, the thermal conductivity and the thermopower of acrylic ACFs with specific surface area (SSA) of $1000\,m^2/g$. The dc conductivity and the photoconductivity were studied by Kuriyama and Dresselhaus [2] over a temperature range of $\sim 30\,K < T < 300\,K$ for phenolic ACFs with SSAs ranging from $1000\,m^2/g$ to $2000\,m^2/g$. The conduction mechanism in disordered solids is generally known to be governed by hopping. Measurement of the electrical conductivity down to temperatures lower than $30\,K$ has been used to identify the hopping conduction model to be used in interpreting the photoconductivity and the magnetoresistance data at higher temperature. A comprehensive understanding of the various transport phenomena should be essential to learning the nature of defects and the role they play in transport. Some knowledge of the microstructure of ACFs can also be obtained from the Raman scattering experiments and such knowledge should help our understanding of the conduction mechanism. It is also interesting to see whether both low-temperature conductivity measurements and Raman scattering can be used as complementary characterization tools for ACFs.

Experimental Details

The precursor materials of the ACFs we studied are isotropic pitch (acryl) and phenol. The SSA ranges from $1000\,m^2/g$ to $3000\,m^2/g$ for the acrylic ACFs and from $1000\,m^2/g$ to $2000\,m^2/g$ for the phenolic ones. The precursor is first spun to form the fiber. Then, the fiber is prepared for activation in an antiflammable process at a temperature of 200 to 400^oC. Finally, the fiber is activated. In the activation process, the fiber is heated in the temperature range 800 – 1200^oC for acrylic fibers and 1100 – 1400^oC for phenolic fibers in O_2, H_2O, CO_2 or other oxidizing atmospheres. The activation process for the phenolic ACFs

Mat. Res. Soc. Symp. Proc. Vol. 209. ©1991 Materials Research Society

used in this paper is described in ref. [3]. The main parameter that characterizes ACFs, the specific surface area (SSA), is controlled by the temperature and the time for activation, the activation process and the precursor materials. It is measured using BET analysis of the adsorption isotherms of N_2 at 78 K and CO_2 at 195 K.

The Raman scattering experiments were performed in the back-scattered configuration. An Argon-ion source was used to provide coherent radiation of less than $100\,mW$ (to avoid sample deterioration due to radiation heating) at a wavelength of $4880\,\mathring{A}$. A two-lens couple was used to focus the beam on the sample at an angle of approximately 40° to the normal. In order that the results be truly characteristic of the type of fibers under study, the laser beam was deliberately defocussed on the sample so that more fibers could be sampled and radiation heating could be avoided. The scattered beam from the sample was collected at normal incidence by a 50-mm camera lens into the entrance slit of a SPEX-1403 monochromator, the setting of which corresponded to a bandpass of $7\,cm^{-1}$. This bandwidth is sufficiently narrow to preserve the lineshape of the broad Raman peaks observed. To avoid fluoresence, we did not use any transparent medium, such as a capillary tube, to hold our samples. Parafilm strips were used in this experiment to wrap the ends of the fibers onto a glass plate which would serve as the sample-holding substrate. The middle part of the fiber bundle was then conveniently exposed to the incident radiation. A good signal-to-noise ratio was obtained when six 25-minute scans were taken for each spectrum.

The transport experiment involved measurements of the resistance of ACFs over a range of temperature spanning $4.2\,K$ to $300\,K$. All resistance measurements were made using the four-point probe method. We used copper wires and silver paint to make contacts with the fiber sample. The contact resistance measured in this experiment was on the order of $10\,\Omega$ typically and was much smaller than the sample resistance ($> 1k\Omega$).

The voltage across the middle contacts was measured by a Keithley model-181 digital nano-voltmeter, whose maximum range was 200-mV, while the current to the fiber was provided by a Keithley model-225 current source. Because the sample resistance could go up to tens of megaohms at low temperature, measurements of such high resistances required a few precautions. First, the current level was adjusted so that the power dissipated in the sample was less than $10^{-7}W$. A resistor of $\sim 10\,M\Omega$, accurately measured by a Keithley model-192 digital multimeter before the experiment, was placed across the input terminals of the nano-voltmeter. At low temperature, it could divert the current from the sample so that the current source could now provide an output current above its minimum range without causing overflow in the nanovoltmeter. The resistor also reduced the total impedance seen by the nanovoltmeter so that a voltage correction was not necessary. Finally, neighbouring samples were placed at least 5 cm apart, a distance observed to be long enough to avoid the problem of signal coupling of two large resistances at low temperature.

A temperature scan from $4.2\,K$ to room temperature took place by natural warming. After the experiment, the resistivity of each sample was calculated using the diameter and length of the sample measured by Scanning Electron Microscopy (SEM).

Experimental Results

Raman measurements were made on a series of samples to examine the effect of SSA, precursor materials and morphology on the Raman spectra. The aim of our study is to correlate disorder with SSA by plotting the appropriate fitting parameters against SSA and to examine the sensitivity of Raman scattering to both the SSA and the precursor materials in strongly disordered systems like ACFs. The ACFs studied include 3 categories, namely acrylic fibers (AC), long phenolic fibers (FRL) and short phenolic fibers (FRS). Although the FRL fibers and the FRS fibers originated from the same precursor, they were treated differently during their activation processes and the resultant degree of disorder in these two types of ACFs could be quite different. FRL fibers are typically more than 10 cm long and

FRS fibers are generally shorter than 1 cm. The AC fibers are pitch-based fibers and were selected in our Raman studies to provide a comparison with the phenol-based fibers, which have a different morphology. Shown in fig. 1 are the Raman spectra for FRL15, FRS15 and AC15 and their corresponding fitting curves. Each of these spectra is typical of all the fibers with different SSAs in the same category. The labels indicate whether the fibers are long phenolic, short phenolic or acrylic ACFs. The numbers in the labels represent the SSA divided by $100\,m^2/g$, so that SSA $= 1500\,m^2/g$ for the ACFs in Fig. 1.

Figure 1: Raman spectra for FRL15 (top figure), FRS15 (middle figure) and AC15 (bottom figure).

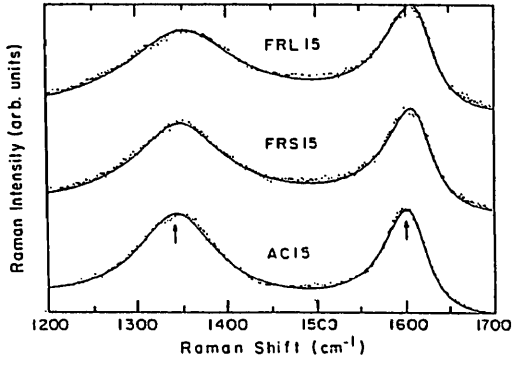

Two peaks were observed in the Raman spectrum for each of the 10 samples studied. The best fit to the data was obtained with a Lorentzian fit to the broad line near $1360\,cm^{-1}$ and a Breit-Wigner-Fano (BWF) lineshape around $1610\,cm^{-1}$. The latter lineshape results from the interaction of a Raman-active continuum with the discrete Raman-allowed mode, which can be identified as the $1582\text{-}cm^{-1}$ E_{2g_2} mode in HOPG. The BWF lineshape was also observed in the Raman spectra for other disordered graphitic systems, such as ion-implanted graphite [4] and stage-1 alkali metal graphite intercalation compounds C_8K, C_8Rb and C_8Cs [5]. The BWF line is described by the following expression:

$$I(\omega) = \frac{I_0[1 + (\omega - \omega_0)/q]^2}{1 + \left[\frac{2}{\Gamma}(\omega - \omega_0)\right]^2} \tag{1}$$

where $I(\omega)$ is the intensity as a function of frequency, I_0 the peak intensity, $1/q$ the interaction between the discrete E_{2g_2} mode and the Raman-active continuum, ω_0 the center position and Γ the full-width-at-half-maximum-intensity (FWHM) of the unweighted Lorentzian (for which $q \to \infty$). The broad peak near $1360\,cm^{-1}$ is disorder-induced, and has also been observed in other disordered graphitic systems such as benzene-derived carbon fibers [6]. In table 1, we list the fitting parameters extracted from the fit to the spectra in Fig. 1. The fitting parameters include the center frequencies, the FWHM's and the relative integrated intensities I_{1360}/I_{1580} for the two peaks observed. Also listed are $1/q$ and Γ_{1580}/q for the Raman-active mode with the BWF lineshape.

The temperature dependence of the dc electrical conductivity of phenolic ACFs is shown in fig. 2. When plotting the logarithm of the conductivity against $1/T$, $1/T^{1/2}$, $1/T^{1/3}$, and $1/T^{1/4}$ for all phenolic ACFs, we found that the plot against $1/T^{1/2}$ appeared most linear over the widest range of temperature. It indicated that the conduction mechanism could be governed by Mott's law in the following form [7]:

$$\sigma(T) = \sigma_0 \exp\left[-\left(\frac{T_0}{T}\right)^{1/p}\right] \tag{2}$$

https://doi.org/10.1557/PROC-209-335 Published online by Cambridge University Press

Table 1: Listed are the fitting parameters (pars.) obtained from fitting a Lorentzian line at $\sim 1350\,cm^{-1}$ and a BWF line at $\sim 1610\,cm^{-1}$ to the data. The numbers in the fiber labels indicate their specific surface area in $100\,m^2/g$.

pars.	FRL10	FRL15	FRL20	FRS12	FRS15	FRS20	AC10	AC15	AC20	AC30
ν_{1360}	1348	1350	1350	1348	1348	1347	1347	1345	1345	1342
Γ_{1360}	152	156	141	120	124	118	114	113	102	103
ν_{1580}	1611	1612	1611	1606	1612	1610	1610	1607	1609	1606
Γ_{1580}	67	64	68	61	61	57	57	57	54	56
$\frac{1}{q}$	-0.23	-0.19	-0.23	-0.10	-0.18	-0.18	-0.17	-0.16	-0.16	-0.17
$\frac{\Gamma_{1580}}{q}$	-15	-12	-16	-6	-11	-10	-10	-9	-9	-10
$\frac{I_{1360}}{I_{1580}}$	1.89	1.90	1.92	1.67	1.69	1.70	1.69	1.81	1.70	1.84

Figure 2: The temperature dependence of the dc electrical conductivity of FRL20 (A), FRS20 (B), FRS12 (C) and FRL10 (D) activated carbon fibers is shown below together with the fitting curves obtained using the model of thermal activation and 2-dimensional VRHC.

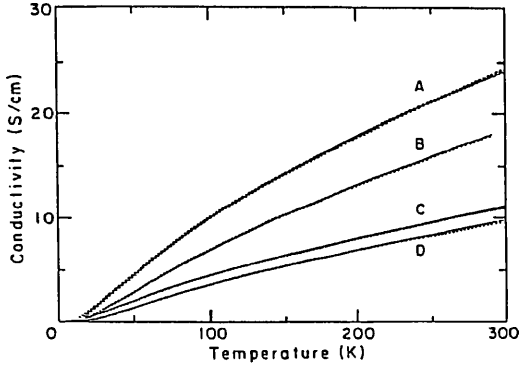

where σ is the conductivity, T_0 a fitting parameter and $p = 2$ in this case. Equation (2) with $p = 2$ can be identified with hopping conduction in the Coulomb gap, which has a parabolic density of states about the Fermi level. The log-log plot of the local activation energy e_a, given by:

$$e_a = \frac{d\,(\ln \rho)}{d((k_B T)^{-1})}\ , \tag{3}$$

where ρ is the resistivity and k_B the Boltzmann constant, versus temperature also yields values of p centered very closely around 2 for all ACFs studied.

However, the conduction mechanism could also be described by Mott's law with different p values and a correction term due to thermal activation. We have least-squares fitted our conductivity data using four different models, namely Coulomb gap conduction, Coulomb gap conduction plus thermal activation, 2-dimensional variable-range hopping conduction (VRHC) plus thermal activation, and lastly 3-dimensional VRHC plus thermal activation. To all these models, we have also added a constant contribution ($\sigma(T = 0)$) to verify that the conductivity is zero at zero temperature. Indeed, $\sigma(T = 0)$ was found to be zero. From table 2, in which we list the least-squares residues for all the models considered, we find that the best fitting model is the 2-d VRHC plus themally activated conduction. The fits are shown in fig. 2. We note that the model of Coulomb gap conduction plus thermal activation is a close competitor and should not be ruled out based on a mere comparison of

https://doi.org/10.1557/PROC-209-335 Published online by Cambridge University Press

least-squares residues, which are affected by the weight allocation to different parts of the data.

Table 2: List of residues resulting from a non-linear least-squares fit of various models to the conductivity data. These models include the Coulomb gap conduction with and without thermal activation, the 3-dimensional variable-range hopping conduction (VRHC) with activation and the 2-dimensional VRHC with activation.

Fiber	FRL10	FRL20	FRS12	FRS20
Coulomb gap	1.35	2.41	2.15	1.74
Coulomb gap + Activation	0.31	0.83	1.07	0.56
2dVRHC + Activation	2.32	0.23	0.25	0.84
3dVRHC + Activation	4.46	0.60	0.50	2.19

Discussion

From table 1, the intensity ratio I_{1360}/I_{1580} is extracted and plotted in fig. 3 against SSA for all ACFs studied. This ratio, together with the other quantities listed in the table,

Figure 3: Plot of the ratio of integrated intensity of the disorder-induced peak to that of the Raman-active peak (I_{1360}/I_{1580}) against SSA for acrylic (AC), long and short phenolic (FRL and FRS) ACFs.

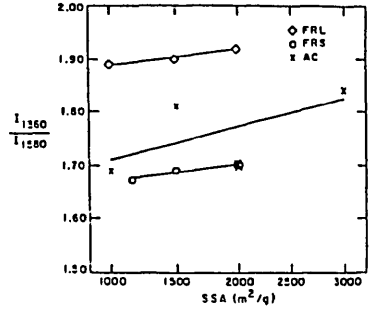

have been used as a measure of the disorder in disordered graphitic systems [6]. The in-plane crystallite size (L_a) is determined by the empirical formula [8]:

$$L_a = 44 \left(\frac{I_{1360}}{I_{1580}}\right)^{-1} \quad (\text{in } \mathring{A}). \tag{4}$$

The intensity ratio in Eq. (4) ranges from 1.67 to 1.92, giving $L_a \simeq 23\text{-}26\,\mathring{A}$. Equation (4) implies that I_{1360}/I_{1580} increases with the disorder in the system. It can then be seen from the plots of Fig. 3 that the FRL fibers are more disordered than the AC fibers, which are in turn more disordered than the FRS fibers, and that there is more disorder in ACFs with a larger SSA, as indicated by the positive slopes of the straight lines resulting from the least-squares linear fit. The slope of the fitting line for the AC fibers is within experimental error of the other slopes. The other quantities in table 1, when similarly plotted against SSA, showed little sensitivity to SSA. While it is still clear from those plots (not shown)

https://doi.org/10.1557/PROC-209-335 Published online by Cambridge University Press

that the FRL fibers are more disordered than both the AC and the FRS fibers, the plots for the AC fibers now lie below those for the FRS fibers, suggesting either that the intensity ratio (I_{1360}/I_{1580}) is not so sensitive a measure of the disorder in a porous system, or that the rest of the quantities are less informative and accurate as a characterization parameter than the intensity ratio.

Looking at fig. 2, one finds that the FRL fibers are more conductive than the FRS fibers and that ACFs with a larger SSA have a higher conductivity than those with a smaller SSA in the same category, in agreement with the other work [2]. In strongly disordered solids, conduction usually occurs by carrier hopping from one localized center to another. The tunneling probability increases with the density of defects, which could be dangling bonds, adsorbed impurity sites or vacancies. The observed trends therefore indicate that the FRL fibers are indeed more disordered than the FRS fibers and that disorder increases with SSA. This finding also encourages us to further our conductivity measurements to include AC fibers in the future to determine whether they are actually more disordered than the FRS fibers.

Based on the least-squares residues, one can argue that the 2-dimensional VRHC is the most likely conduction mechanism at low temperature. However, since the estimated hopping distance is larger than L_a, it is questionable whether the hopping carriers should see a 2-dimensional structure at all. Although the log-log plot of the local activation energy versus temperature suggests that Coulomb gap conduction could be present, the localization length and the pseudo-gap width were both found to be unconvincingly large (360 $\AA$ and $\sim 1\,eV$, respectively). Therefore, we cannot yet conclude convincingly which conduction mechanism governs the electrical transport of ACFs at low temperature.

Acknowledgement

We would like to express our gratitude to Dr. D. E. Heiman of the National Magnet Lab., M.I.T., for generously allowing us to use his optical equipment. We treasure the many enlightening discussions with Mr. di Vittorio of the Dept. of Materials Science at M.I.T. We would also like to acknowledge the Lawrence Livermore National Laboratory for support of this work under subcontract B130530.

References

[1] S. L. diVittorio, to be published (1990).

[2] K. Kuriyama and M. S. Dresselhaus, to be published (1990).

[3] E. Tanaka, Fuel and Combustion, 54(4), 241 (1987).

[4] B. S. Elman, M. S. Dresselhaus, G. Dresselhaus, E. W. Maby, and H. Mazurek, Phys. Rev. B, 24(2), 1027 (1981).

[5] M. S. Dresselhaus and G. Dresselhaus, in Light Scattering in Solids III, Topics in Applied Physics, Vol. 51, edited by M. Cardona and G. Güntherodt (Springer-Verlag, Berlin, 1982), p. 3.

[6] T. C. Chieu, M. S. Dresselhaus, and M. Endo, Phys. Rev. B, 26(10), 5867 (1982).

[7] N. F. Mott, Conduction in Non-Crystalline Materials (Oxford University Press, New York, 1987).

[8] D. S. Knight and W. B. White, J. Mater. Res., 4(2), 385 (1989).